

# 1 Effect of water depth and swell parameters on 2 wave propagation in the coastal zone of Benin

3  
4  
5  
6

## 7 ABSTRACT

8

The coastal zone is studied as a morphodynamic system in the present work. A morphodynamic system comprises a geomorphological entity that adjusts its morphology in response to variations in a dynamic component. In recent years, particularly from 2015 to 2016, strong swells have been observed and have induced the destruction of coastal infrastructure and strong coastal erosion in the Gulf of Guinea, particularly Benin. Following this observation, our study is carried out to understand the origin of these strong events. Through this work, we tried to highlight the effect of water depth and swell parameters on wave propagation using experimental models from the literature. For this reason, MATLAB and Mathematica software were used for simulations. It can be said from the results obtained that the wave height has a considerable effect on the wave profile. The variation in water depth as a function of distance from the bed shows that it significantly affects the wave and its components.

9

10 **Keywords:** Wave simulation; Water depth; Swell and Wave propagation; Benin coastal zone

11

## 12 SCIENTIFIC NOTATION TABLES

13  $v$  : Ocean water flow Velocity (m/s) ;

14  $\rho$  : Density of sea water ( $\text{kg/m}^3$ ) ;

15  $\Phi$  : Velocity potential in the ocean ( $\text{m}^2/\text{s}$ ) ;

16  $\eta$  : Vertical elevation of the water level relative to the reference (m) ;

17  $\beta$  : Inclination of the seabed relative to the horizontal (rad) ;

18  $\Upsilon$  : Hydrodynamic pressure (Pa) ;

19  $g$  : Acceleration of gravity ( $\text{m/s}^2$ ) ;

20  $H$ : Crest-to-trough height of the swell (m) ;

21  $H_0$ : Crest-to-trough height of the offshore swell (m) ;

22  $H_d$ : Crest-to-trough height of the swell at the breaking point (m) ;

23  $H_s$  : Significant crest-to-trough swell height (m) ;

24  $H_{max}$ : Maximum crest to trough height of the swell (m) ;

25  $H_{min}$ : Minimum crest-to-trough wave height (m) ;

26  $T_m$ : Average swell period (s) ;

27  $T_p$ : Peak wave period (s) ;

28  $L = \frac{2\pi}{k}$ : Wavelength of the swell (m) ;

29  $T = \frac{2\pi}{\omega}$ : Swell period (s) ;

30  $d$  : Near sea surface-bottom distance in coastal zones (m) ;

31  $\vec{r}$ : Position vector of a point located on the free surface;

32  $V_g$ : Group swell Velocity (m/s) ;

33  $V_\phi$ : Swell phase Velocity (m/s) ;

34  $V_x$  : Horizontal Velocity of the water particles struck by the swell;

35  $V_z$  : Vertical Velocity of the water particles struck by the swell;

36  $K_R$  : Refraction coefficients;  
37  $K_S$  : Shoaling coefficients;  
38  $A_x$  : Horizontal accelerations of water particles struck by the swell;  
39  $A_z$  : Vertical acceleration of water particles struck by the swell;  
40  $\mathcal{L}_x$  : Horizontal movement of water particles struck by the swell;  
41  $\mathcal{L}_z$  : Vertical movement of water particles hit by the swell;;  
42 MCA : Millenium Challenge Account.

43  
44

## 45 1. INTRODUCTION

46 Comprehensive theoretical research on the propagation of waves in Benin's coastal  
47 areas could yield vital information for the region's coastal risk management and planning. [1].  
48 The study of swell and wave propagation in the coastal zone of Benin involves  
49 understanding various factors that influence wave behavior, such as wind patterns, local  
50 water depth, coastal morphology, fetch, tide, ocean currents, and oceanographic  
51 conditions[2]. A theoretical study typically involves mathematical modeling and simulation to  
52 predict wave characteristics along the coast of Benin. Studying the ocean as a whole  
53 requires bridges linking the transversal skills of the different sciences in this case theoretical  
54 physics through modeling and analysis which lead to understanding and the search for  
55 solutions to the consequences of the increase in the level of the sea[1]. Mathematical  
56 theories, at the basis of all theoretical knowledge of the physical functioning of our  
57 environment, which deal with waves, have developed and become more complex. They  
58 represent many phenomena linked to waves based on hypotheses developed from the  
59 general equations of fluid mechanics, and now make it possible to study ever more  
60 sophisticated problems analytically and numerically[3]. Overall, a theoretical study on swell  
61 and wave propagation in the coastal zone of Benin requires a multidisciplinary approach  
62 integrating oceanography, meteorology, hydrodynamics, and coastal engineering to provide  
63 valuable information for coastal management and decision-making[4]. The most spectacular  
64 physical manifestation occurring in the ocean is undoubtedly the swell. The coastline of  
65 Benin has suffered severe erosion for several years[5]. This phenomenon could be  
66 explained by a hydrodynamic dominated mainly by swells generated by the winds as well as  
67 a sandy coastline subject to a local microtidal type tide and a seasonal evolution of the  
68 intensity of the swells. In short, the coast of Cotonou in Benin is subject to two swell regimes:  
69 short swells (less energetic) generated by local winds and long swells (very energetic)  
70 generated in the South Atlantic which are the engine of one of the most significant coastal  
71 drifts in the world, from west to east[6]. In Cotonou, coastal transit is caused by the oblique  
72 attack of north-east or east-north-east swells during different storms [5]. Under the action of  
73 currents, winds, or swells, the solid particles, that form the sediments encountered in rivers  
74 and along coastlines, can be torn from the seabed, suspended, or transported over  
75 distances. More or less large and deposited in calm areas. These interactions are extremely  
76 complex in nature and the sedimentary movements that can be observed depend on multiple  
77 parameters. Velocity gradients in the fluid, vortices, bottom geometry, bank lines, nature of  
78 materials, thickness on the bedrock, porosity, and cohesion of the deposits, characteristics  
79 of the fluid... Will intervene in the conditions of erosion and transport of the materials. All  
80 these parameters, in addition, will not be constant over time but will undergo fluctuations.  
81 The swell in the fluid mass will cause the sediments to flow in certain situations in a mass  
82 direction toward privileged sectors due to reactions from translational and compensatory  
83 currents, return currents, orbital movements on the seabed, and coastal or return currents.  
84 On the sea surface, the friction of the local wind causes the water surface to move and  
85 generate ripples[1], [7]. This 'sea of wind' is the superposition of several sinusoidal waves,  
86 forming 'irregular' waves[2], [4]. Under the effect of pressure gradients associated with  
87 gravity and induced by these variations in water height, these waves then propagate and are

88 called gravity waves, or surface waves. These waves turn into swells when they propagate.  
89 The swell is thus the part of the sea state characterized by its absence of a relationship with  
90 the local wind. As part of this study, no distinction will be made between swell and waves,  
91 these two terms will define the sea state arriving on the shore. The land-sea interface is an  
92 extremely fragile environment. Coastlines, interfaces between land and sea, are places of  
93 great biological and landscape diversity, subject to strong pressures from natural elements  
94 and human beings. In the coastal zone, the most dynamic zones are the internal surf and  
95 swash zones[5]. The swash zone is of fundamental importance in the study of the coastal  
96 zone. The internal surf zone thus represents the border between the emerged part of the  
97 beach and the breaking zone. The internal surf zone and the swash zone thus form the very  
98 last zone of the beach where the waves will dissipate or reflect their remaining energy[1],  
99 [8]. Throughout the world, coastlines are threatened by the combination of a multitude of  
100 factors, sometimes natural and most often anthropogenic. Thus, to the local disturbances  
101 caused to coastal areas by port infrastructures, dams, sediment collection from the beach, or  
102 even urban expansion, are added the global consequences of climate change, including the  
103 certain rise in the level of oceans and the probable amplification of devastating marine  
104 weather conditions. The direct consequence of global warming, the rise in ocean levels will  
105 have obvious consequences on coastal erosion in the decades to come. It is thus estimated,  
106 on a global scale, that sea levels could rise between 10 and 25 cm over the last century and  
107 28 and 98 cm by 2100 according to estimates from the IPCC (Intergovernmental Panel on  
108 Climate Change). Climate change presented in their ar5 assessment report, based on  
109 different warming scenarios (IPCC, 2014)[1], [8]. In Cotonou, since 2011, it was recently  
110 calculated that the average increase in sea level was 3.2 mm year<sup>-1</sup>, which is close to the  
111 global values obtained over a similar period (IPCC, 2014)[9]. The simplest mathematical  
112 representation assuming the water waves used for the simulation is given as follows: two-  
113 dimensional (2-D), small amplitude, sinusoidal, and progressively definable by their  
114 amplitude and wave period in a depth of water given. In the simple representation of  
115 swells/waves, the movements and displacements of swell/wave, the kinematics (i.e.,  
116 velocities and accelerations of swell/wave), and the dynamics (i.e. (i.e., wave/wave pressure  
117 and resultant forces and moments) are determined for technology design evaluations. When  
118 the wave amplitude becomes larger, simple treatment cannot be scaled. For regular  
119 swell/wave, we consider the 2-D approximation of the ocean surface deviated from a pure  
120 sinusoid [8]. This representation requires more complicated mathematical theories. These  
121 theories become non-linear and allow the formulation of swells/waves that are not sinusoidal  
122 in shape; for example, flat troughs and sharp ridges in shallow water when swells/waves are  
123 relatively high. The simplest swell/wave theory is first order and small amplitude, or the airy  
124 theory which is called the linear theory[3]. This representation requires more complicated  
125 mathematical theories.

126

## 127 **2. MATERIAL AND METHODS**

### 128 **2.1 Presentation of the study site**

129



**Figure 1a:** Geographical location of the coastal zone of Benin in the Gulf of Guinea

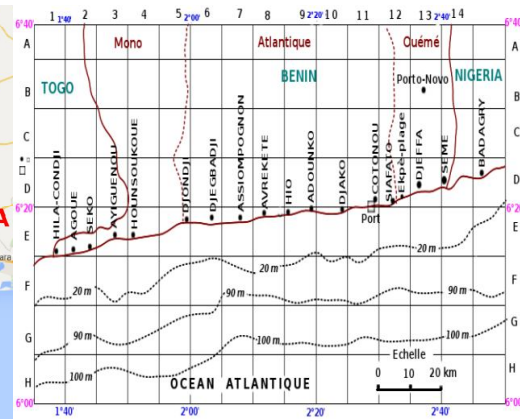


**Figure 1b:** Bathymetric map of the Benin coastal zone



**Figure 1c:** Image of Benin's coastal strip

130  
131  
132  
133  
134  
135  
136  
137  
138  
139  
140  
141  
142  
143  
144  
145  
146  
147  
148  
149

The coastal zone of Benin, between  $6^{\circ}15'$  and  $6^{\circ}38'$  north latitude, is part of the coastal sedimentary basin, the oldest of which dates back to the Cretaceous. Benin is a coastal state in the Gulf of Guinea (**figure 1a**). The coastline generally presents weak concavities oriented towards the ocean on this coast. There is increasing erosion towards the east. The climate is subequatorial with two dry seasons and two rainy seasons [4], [8], [10]. In the coastal zone of Benin, there is no major obstacle that could significantly modify the direction of wave propagation ( $\theta \approx \theta_0$ ) [8]. The average slope in the shoaling zone on this site is  $p = \tan\beta \approx \frac{90}{2000} = 0,045$ [2] (**Figure 1b**). In Benin, the swells which propagate towards the coast have a period  $T$  which varies between  $10\text{ s}$  and  $14\text{ s}$  and whose peak period is  $T_p = 11.50\text{ s}$ . Experimental measurements have shown that these waves break at the point of local depth  $d_b$  such that  $4\text{ m} \leq d_b \leq 5\text{ m}$  and that their period oscillates between  $9\text{ s}$  and  $15\text{ s}$ [11]. Their heights vary almost sinusoidally and have two maxima and two minima on the same day. These heights vary between  $0.6\text{ m}$  and  $1.4\text{ m}$ . The maxima are observed around  $5\text{ a.m}$  and  $5\text{ p.m}$  GMT and the minima around  $00\text{ a.m}$  and  $12\text{ p.m}$ [12]. From data measurements relating to swell carried out at the autonomous port of Cotonou, at time intervals of five minutes over four consecutive years (June 2015 to April 2016) and obtained from the Institute of Fisheries and Oceanographic Research of Benin (IRHOB) of the Beninese Center for Scientific and Technical Research (CBRST), we have:

- Performs analysis of wave statistics on the coast of Benin.

- 150 ➤ Simulated the temporal evolution of wave parameters such as the significant height  $H_s$  (m),  
 151 the period of the peak  $T_p$  (s) and the direction of the peak  $Dir$  (°).  
 152 ➤ Shown the evolution of the vertical elevation  $\eta$  of the sea surface as a function of local water  
 153 depth and compare swell profiles as a function of time in the different areas. For the study of  
 154 swell propagation on this site, the abscissa axis is oriented in the East-West direction and the  
 155 ordinate axis in the North-South direction as shown in **Figure 2** below:

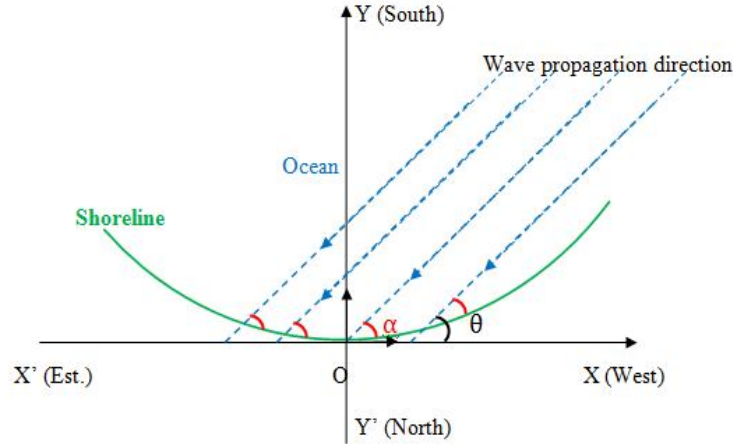


**Figure 2:** Schematization of the study benchmark and direction of wave propagation in Benin coastal zone.

156  
 157 The coastal strip of Benin is oriented in the South-West-West direction and thus tilts at an  
 158 angle  $\theta_o = 20^\circ$  approximately about the West-East direction [4].  
 159

## 2.2. Equations to solve the problem

- The movement of fluids (air and ocean) obeys the following Navier-Stokes equation [7].

$$162 \frac{\partial \vec{v}_i}{\partial t} + (\vec{v}_i \cdot \nabla) \vec{v}_i + \frac{1}{\rho_i} (\nabla P_i) - \vec{g} - \frac{\mu}{\rho_i} (\nabla^2 \vec{v}_i) = \vec{0} \text{ with } i = 1, 2 \quad (1)$$

163 Irrotational and incompressible coastal flow can be modeled using Euler's equations in 3  
 164 dimensions. The strong non-linear nature of these equations prevents us from directly applying a  
 165 numerical solution method. We must therefore simplify them before applying a numerical  
 166 scheme. The viscosity in these two media being very negligible [13] and for surface waves, the  
 167 convective term is negligible ( $\mu \ll \rho_i$ ) compared to the acceleration  $(\vec{v}_i \cdot \nabla) \vec{v}_i \ll \frac{\partial \vec{v}_i}{\partial t}$  [1].

168 The oceanic environment is an incompressible fluid ( $div(\vec{v}) = 0$ ), the flow is potential ( $\vec{v} = \vec{\nabla} \phi$ )  
 169 and for a perfect fluid, we show that an irrotational disturbance remains so indefinitely. We can  
 170 apply this theorem to the movement of waves whose flow will be assumed to be zero rotational  
 171 (irrotational)  $\text{rot}(\vec{v}) = \vec{0}$  [1] where  $\vec{v}$  is the speed of a water particle driven by the flow and  $\phi_2 = \phi$  the  
 172 scalar potential of the velocities in the ocean and  $\phi_1$  that of the atmosphere. Thus, we obtain the  
 173 Laplace equation below [14]  $\Delta \phi = 0$ . The solution of equation (1) allows us to find the dynamic  
 174 pressure  $Y$  [15].

$$175 Y = -\rho \left( \frac{\partial \phi}{\partial t} \right) \quad (2)$$

- The area in which the effect of the Airy or Stokes swell (swell of very small amplitude compared to their wavelength) is felt is such [15], [16].

$$178 \begin{cases} -\infty \leq x \leq +\infty \\ -\infty \leq y \leq +\infty \\ -d \leq z \leq 0 \end{cases} \quad (3)$$

- A water particle at a point on the free surface has a vertical speed  $v_z = \frac{\partial \eta}{\partial t}$  along the vertical axis. The kinematic condition in  $z = \eta$  gives [7].

180

$$181 \quad \left(\frac{\partial \phi}{\partial z}\right)_{(z=\eta)} = \left(\frac{\partial \phi_i}{\partial z}\right)_{(z=\eta)} = \frac{\partial \eta}{\partial t} \quad (4)$$

182 • The swell being a surface wave, its effect disappears after a certain depth ( $z = -d$ ). The  
183 condition of non-penetration to the bottom amounts to [2], [8].

$$184 \quad v_z(z = -d) = 0 \Rightarrow \left(\frac{\partial \phi}{\partial z}\right)_{(z=-d)} = 0 \quad (5)$$

185 • The dynamic condition at  $z = \eta$  due to the existence of pressure and gravity forces at  
186 altitude  $z$  is written [15], [16].

$$187 \quad \left[ g\eta + \frac{\partial \phi}{\partial t} \right]_{z=0} = 0 \Rightarrow \left[ \frac{\partial^2 \phi}{\partial t^2} + g \frac{\partial \phi}{\partial z} \right]_{z=0} = 0 \quad (6)$$

188 • The direction of wave propagation is almost rectilinear. It is assimilated to the axis  $(O, \vec{i})$  and  
189 the average vertical elevation of the free surface is zero over a period.

$$190 \quad \int_t^{t+T} \eta(\vec{r}, t) dt = \int_x^{x+L} \eta(\vec{r}, t) dx = 0 \quad (7)$$

191 • Any swell of wavelength propagates through three particular zones [16], [17]. Offshore  
192 (deep water) when  $d > \frac{L}{2}$ ; the lifting zone (Shoaling zone) if  $\frac{L}{25} \leq d \leq \frac{L}{2}$ ; the breaking zone or  
193 shallow waters (Surf and Swash zones) for  $0 \leq d \leq \frac{L}{25}$

194 • On the Beninese coast, the average slope in the Shoaling zone [2], [12] is :

$$195 \quad p = \tan(\beta) = \frac{90}{2000} = 0,045(8)$$

196 According to the bathymetric map along the Beninese maritime coast (**Figure 2b**) shows us that  
197 there is very little variation in the wavelength of the swells, either:

$$198 \quad L = \frac{2\pi}{k} = \frac{gT^2}{2\pi} (9)$$

### 199 **2.3. Expression of $\phi(\vec{r}, t)$ , $\eta(\vec{r}, t)$ and the group velocity $V_g$**

200 Solving equation (1) with conditions (3), (4), (5) and (6) gives complex results of which only  
201 the real parts below reflect the physical phenomenon [18], [19].

$$202 \quad \begin{cases} \phi_1 = \phi_1(x, y, z, t) = \frac{gH}{2w} e^{kz} \sin(\vec{k} \cdot \vec{r} - \omega t) \\ \phi_1 = \phi_1(x, y, z, t) = \frac{gH \cosh[k(z+d)]}{2w \cosh(kd)} \sin(\vec{k} \cdot \vec{r} - \omega t) \\ \eta = \eta(x, y, t) = \eta_0 \cos(\vec{k} \cdot \vec{r} - \omega t) = \frac{H}{2} \cos(\vec{k} \cdot \vec{r} - \omega t) \\ Y = -\rho \frac{\partial \phi}{\partial t} = \frac{\rho g H \cosh[k(z+d)]}{2 \cosh(kd)} \cos(\vec{k} \cdot \vec{r} - \omega t) \end{cases} \quad (10)$$

203 The fluid velocity in the x direction is:  $V_x = \frac{\partial \phi}{\partial x}$  and the fluid velocity in the z direction is:  $V_z = \frac{\partial \phi}{\partial z}$ .

204 The positions, velocities and accelerations of local fluids are:

$$205 \quad \vec{V} \begin{cases} V_x = \frac{gHT}{2L} \frac{\cosh[2\pi(z+d)/L]}{\cosh(2\pi d/L)} \cos(\theta) \\ V_z = \frac{gHT}{2L} \frac{\sinh[2\pi(z+d)/L]}{\cosh(2\pi d/L)} \sin(\theta) \end{cases} \text{ with } \theta = \frac{2\pi x}{L} - \frac{2\pi t}{T}$$

206 (11)

207 The integration of this equation (11) gives the equations that parameterize the position of a water  
208 particle struck by the swell.

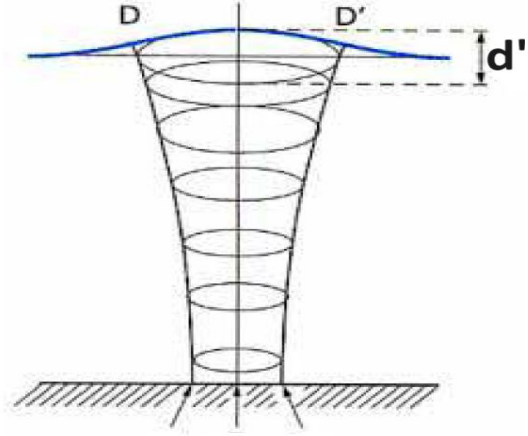
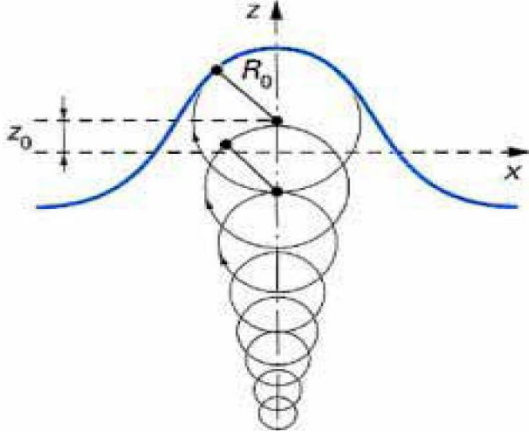
$$209 \quad \vec{OM} \begin{cases} X = \frac{H}{2} \frac{\cosh[2\pi(z+d)/L]}{\cosh(2\pi d/L)} \sin(\theta) \\ Z = \frac{H}{2} \frac{\sinh[2\pi(z+d)/L]}{\cosh(2\pi d/L)} \cos(\theta) \end{cases} \text{ with } \theta = \frac{2\pi x}{L} - \frac{2\pi t}{T}$$

210 (12)

211 These equations express water particles' velocity and position components at any  
212 distance  $(z + d)$  above the bottom. They are periodic in  $x$  and  $t$ . For a given value of the phase  
213 angle  $\theta = 2\pi \left( \frac{x}{L} - \frac{t}{T} \right)$ . The trajectory of the particles is therefore circular in infinite depth  
214 (offshore) and elliptical in shape that becomes more and more crushed as the bottom rises. The

215 equations of system (11) generally parameterize the ellipses with major horizontal axis DD' and  
 216 minor vertical axis d' verifying the equation:

$$217 \quad \left(\frac{x}{DD'}\right)^2 + \left(\frac{z}{d'}\right)^2 = 1 \quad \text{with} \quad \begin{cases} DD' = \frac{H \cosh[2\pi(z+d)/L]}{2 \cosh(2\pi d/L)} \\ d' = \frac{H \sinh[2\pi(z+d)/L]}{2 \cosh(2\pi d/L)} \end{cases} \quad (13)$$



218 **Figure 3a:**Trajectory of water particles in  
 219 Gerstner swell [20], [21]

218 **Figure 3b:**Trajectory of water particles in  
 219 Stokes swell [21], [21]

218 This model established in 1804 by Gerstner is a rigorous solution for a fluid at infinite depth  
 219 (**Figure 3a**). Each fluid particle is supposed to rotate around a point with coordinates  $X_0, Z_0$ ,  
 220 describing a circumference of radius  $R$ , decreasing exponentially with depth  $d$ .  
 221 The derivation of this equation (11) gives the equations that parameterize the accelerations of the  
 222 particles of the fluid struck by the swell. The accelerations of the fluid particles are:

$$223 \quad \begin{cases} A_x = \frac{g\pi H}{L} \frac{\cosh[2\pi(z+d)/L]}{\cosh(2\pi d/L)} \sin(\theta) \\ A_z = -\frac{g\pi H}{L} \frac{\sinh[2\pi(z+d)/L]}{\cosh(2\pi d/L)} \cos(\theta) \end{cases} \quad \text{with} \quad \theta = \frac{2\pi x}{L} - \frac{2\pi t}{T} \quad (14)$$

226 And the movement of water particles is given by:

$$227 \quad \begin{cases} \mathcal{L}_x = -\frac{HgT^2}{4\pi L} \frac{\cosh[2\pi(z+d)/L]}{\cosh(2\pi d/L)} \sin(\theta) \\ \mathcal{L}_z = \frac{HgT^2}{4\pi L} \frac{\sinh[2\pi(z+d)/L]}{\cosh(2\pi d/L)} \cos(\theta) \end{cases} \quad \text{with} \quad \theta = \frac{2\pi x}{L} - \frac{2\pi t}{T} \quad (15)$$

228 The secondary external pressure under a wave is the sum of two pressure components,  
 229 dynamic and static, and is given by:

$$230 \quad Y' = \frac{\rho g H}{2} \frac{\cosh[2\pi(z+d)/L]}{\cosh(2\pi d/L)} \cos(\theta) - \rho g z + p_0 \quad \text{with} \quad \theta = \frac{2\pi x}{L} - \frac{2\pi t}{T} \quad (16)$$

233 The equation for the water surface is given by:

$$234 \quad \eta = \eta_1 + \eta_2 = \frac{H}{2} \cos\left(\frac{2\pi x}{L_1} - \frac{2\pi t}{T_1}\right) + \frac{H}{2} \cos\left(\frac{2\pi x}{L_2} - \frac{2\pi t}{T_2}\right) \quad (17)$$

235 and

$$236 \quad \eta_{enveloppe} = \pm H \cos\left[\pi \left(\frac{L_2 - L_1}{L_1 L_2}\right) x - \pi \left(\frac{T_2 - T_1}{T_1 T_2}\right) t\right] \quad (18)$$

237 The swell dispersion relation according to the linear theory[22], [23] is :

$$238 \quad \omega^2 = gk \tanh(kd) \quad (19)$$

239 The phase (celerity) and group velocities of a swell are respectively[17], [24].

$$\begin{cases} V_\varphi = \frac{\omega}{k} = \sqrt{\frac{g}{k} \tanh(kd)} \\ V_g = \frac{\partial \omega}{\partial k} = \frac{1}{2} \frac{\omega}{k} \left( 1 + \frac{2kd}{\sinh(2kd)} \right) \end{cases} \quad (20)$$

Note that an argument of the hyperbolic tangent  $kd = 2\pi d/L_0$  is large, the  $\tanh(kd)$  approaches 1, and for small values of  $kd$ ,  $\tanh(kd) \simeq kd$ . Water waves are classified in Table 1 based on the relative depth criterion  $d/L_0$ .

Classification	$\mu = d/L_0$	$kd$	$\tanh(kd)$
Deep Waters	1/2 to $+\infty$	$\pi$ to $+\infty$	= 1
Shoaling zone	1/25 to 1/2	$\pi/10$ to $\pi$	$\tanh(kd)$
Shallow waters	0 to 1/25	0 to $\pi/10$	= $kd$

**Table 1** :Waves classification

In deep waters,  $V_{g_0} = \frac{1}{2} V_\varphi = \frac{gT}{4\pi} \text{gold} L_0 = \frac{gT^2}{2\pi}$  [25] ;

In the Shoaling zone,  $V_g = \frac{1}{2} \left( 1 + \frac{2kd}{\sinh(2kd)} \right) \sqrt{\frac{g}{k} \tanh(kd)}$  ;

In the shallow waters,  $V_g = V_\varphi = \sqrt{gd}$  [26] ;

In the end, we have:

$$V_g(d) = \begin{cases} \frac{gT}{4\pi} \text{if } \frac{d}{L_0} > \frac{1}{2} \\ \frac{1}{2} \left( 1 + \frac{2kd}{\sinh(2kd)} \right) \sqrt{\frac{g}{k} \tanh(kd)} \text{if } \frac{1}{25} \leq \frac{d}{L_0} \leq \frac{1}{2} \\ \sqrt{gd} \text{if } 0 \leq \frac{d}{L_0} \leq \frac{1}{25} \end{cases} \quad (21)$$

Gold by posing  $k = 2\pi/L_0$

$$V_g(d) = \begin{cases} \frac{gT}{4\pi} \text{if } \frac{d}{L_0} > \frac{1}{2} \\ \frac{1}{2} \left( 1 + \frac{4\pi d/L_0}{\sinh(4\pi d/L_0)} \right) \sqrt{\frac{gL_0}{2\pi} \tanh(2\pi d/L_0)} \text{if } \frac{1}{25} \leq \frac{d}{L_0} \leq \frac{1}{2} \\ \sqrt{gd} \text{if } 0 \leq \frac{d}{L_0} \leq \frac{1}{25} \end{cases} \quad (22)$$

## 2.4.Swell height

In deep water, the swell height is constant and is  $H = H_0 = cste$ .  
In the Shoaling zone [7], [8],  $H = K_S K_R H_0$  Where

$$K_S = \sqrt{\frac{V_{g^0}}{V_g}} = \left( \frac{2\pi d/L_0}{\cosh^2(2\pi d/L_0)} + \tanh(2\pi d/L_0) \right)^{\frac{1}{2}} \text{and} \quad K_R = \sqrt{\frac{\cos\theta_0}{\cos\theta}} \quad (23)$$

Are respectively the Shoaling and refraction coefficients,  $\theta_0$  and  $\theta$  the directions of propagation of the wave before and after refraction. So we get, [12] :

$$H = H_0 \sqrt{\frac{\cos\theta_0}{\cos\theta}} \left( \frac{2\pi d/L_0}{\cosh^2(2\pi d/L_0)} + \tanh(2\pi d/L_0) \right)^{\frac{1}{2}} \quad (24)$$

The height of the swell decreases in the breaking zone [5], [21] and According to P. Bonneton (2002), this height is given by:

In the end, we have:

$$H(d) = \begin{cases} H_o & \text{if } \frac{d}{L_0} > \frac{1}{2} \\ H_o \sqrt{\frac{\cos\theta_0}{\cos\theta}} \left( \frac{2\pi d/L_0}{\cosh^2(2\pi d/L_0)} + \tanh(2\pi d/L_0) \right)^{-\frac{1}{2}} & \text{if } \frac{d_b}{L_0} \leq \frac{d}{L_0} \leq \frac{1}{2} \\ H_o \left[ \frac{2H_o}{T \tan\beta \sqrt{gd_b}} \left( \frac{d}{d_b} \right)^{-1/2} + \left( 1 - \frac{2H_o}{T \tan\beta \sqrt{gd_b}} \right) \left( \frac{d}{d_b} \right)^{1/4} \right]^{-1} & \text{if } 0 \leq d \leq d_b \end{cases} \quad (25)$$

267  
268  
269

### 270 3. RESULTS AND DISCUSSION

#### 271 3.1. Results

272 > The curves in **Figure 4** reveal the temporal distribution of the hydrodynamic  
273 parameters of the port of Cotonou from 2015 to 2016. The data observed every hour of the  
274 parameters characterizing the state of the waves (significant height, peak direction, and peak  
275 period) at both anchorages from December 2015 to August 2016 are presented in **Figure 4**.

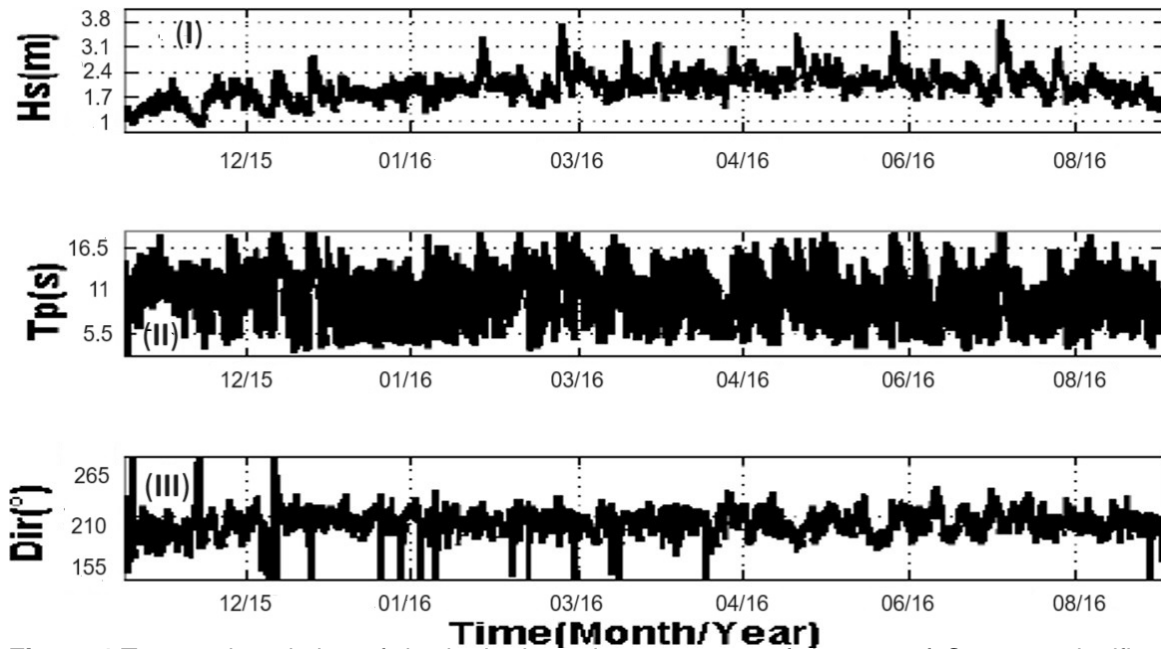


**Figure 4:**Temporal evolution of the hydrodynamic parameters of the port of Cotonou: significant wave height (Hs) (I), peak period (Tp) (II), and direction (Dir) (III) between 2015 and 2016.

276 > The following Figure 5 shows us the comparison of wave profiles and physical quantities as a  
277 function of time.  
278

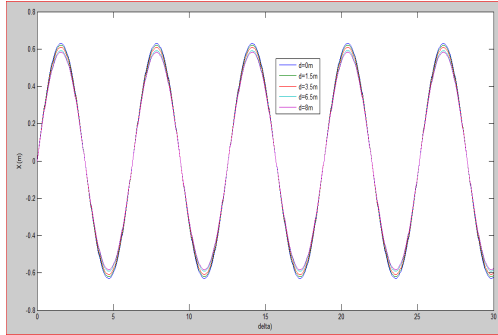


**Figure 5a:**Variation of horizontal position X

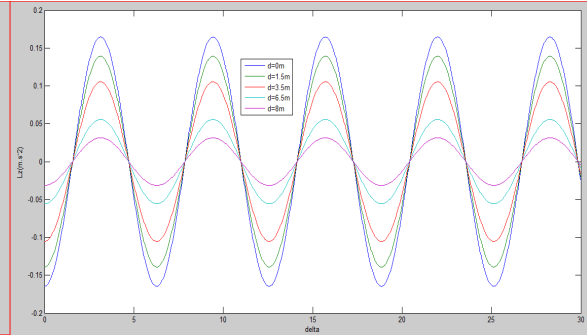


**Figure 5b:**Variation of vertical position Z

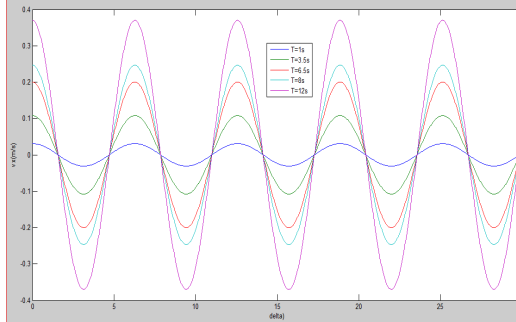


**Figure 5c:**Variation of the horizontal velocity of water particles

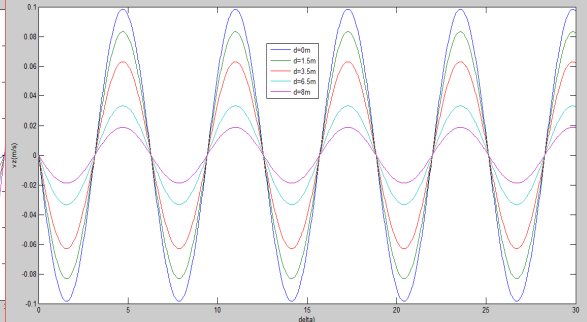


**Figure 5d:**Variation of the vertical velocity of water particles

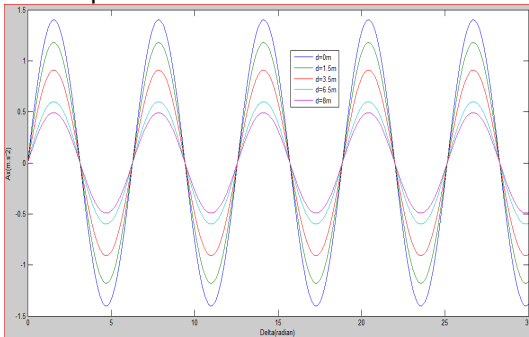


**Figure 5e:**Variation of horizontal acceleration of water particles

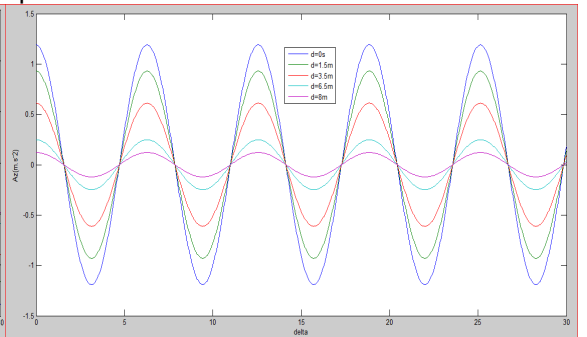


**Figure 5f:**Variation of vertical acceleration of water particles

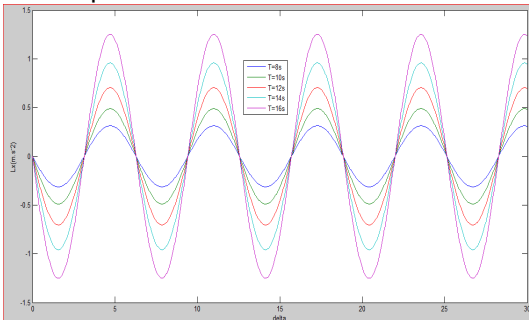


**Figure 5g:**Variation in horizontal displacement of water particles to  $d=cst$

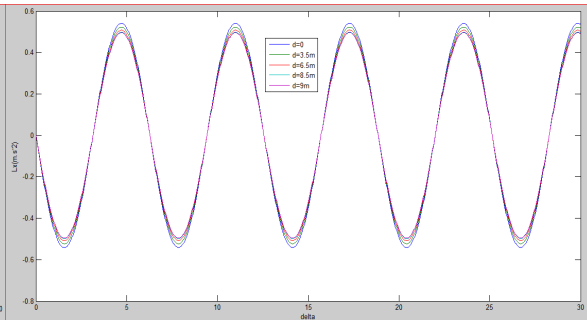


**Figure 5h:**Variation in horizontal displacement of water particles to  $T=cst$

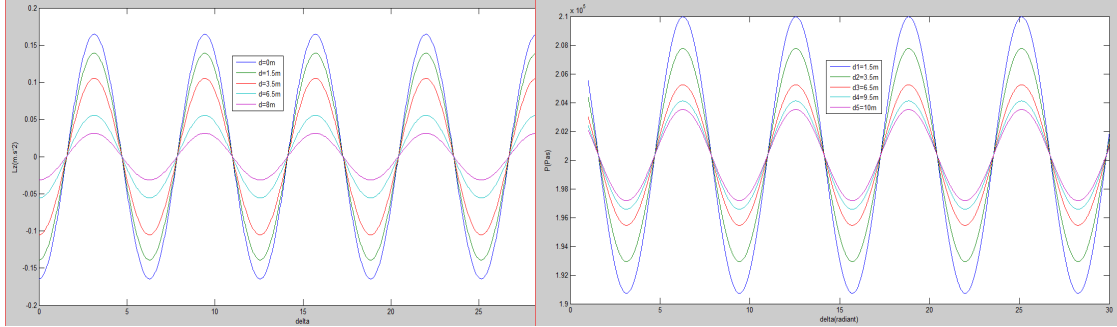
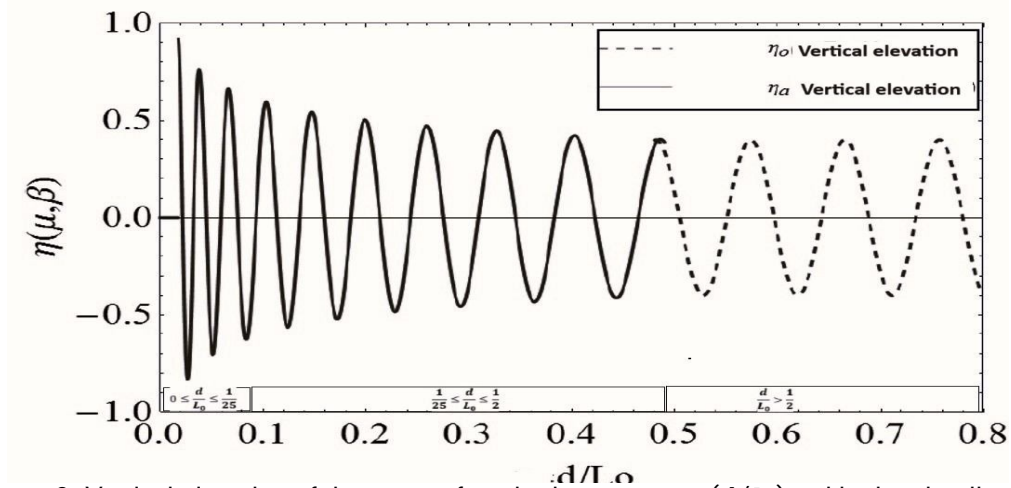


**Figure 5i:**Variation of vertical displacemen **Figure 5j:**Variation of dynamic pressure water particles

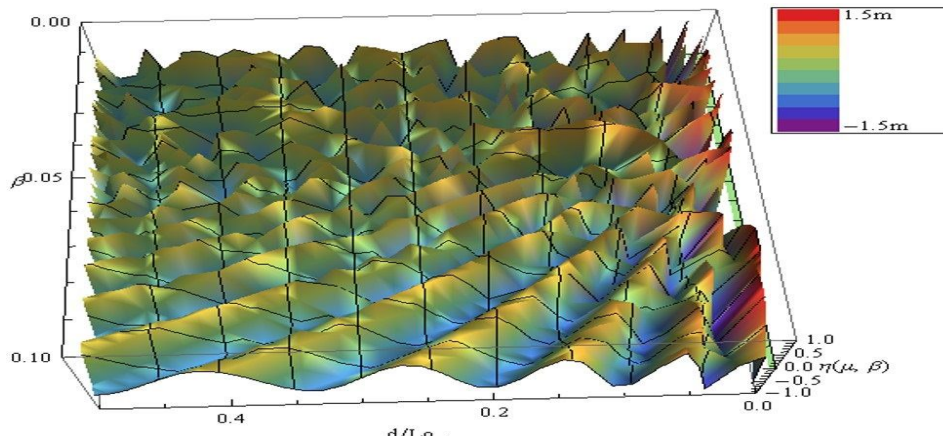
279  
280  
281  
282  
283

➤ **Figures 6,6a, and 6b,** show the evolution of the vertical elevation of the sea surface as a function of the local water depth  $\mu$  and the slope of the seabed  $\beta$ . The curve in **Figure 6** is a representation in dimension 2 (2D) whereas those of **Figures 6a** and **6b** are its representations in dimension 3 (3D).



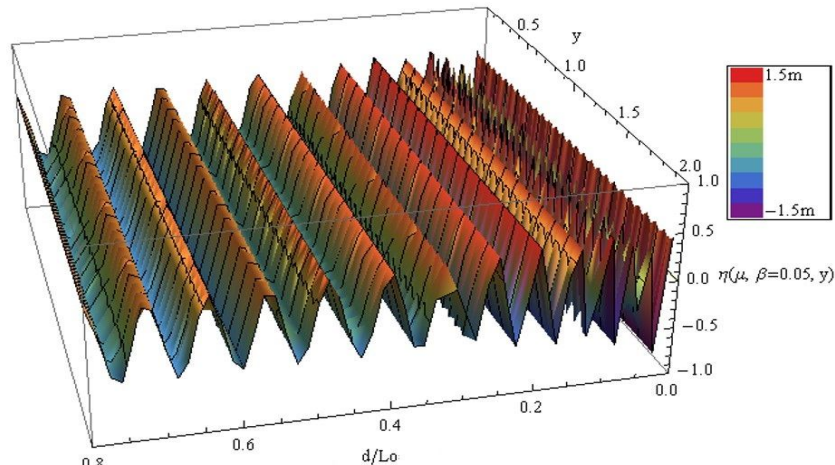
284  
285  
286  
287

**Figure 6:** Vertical elevation of the sea surface in deep water  $\eta_0(d/L_0)$  and in the shoaling zone  $\eta_a(d/L_0, \beta)$  in dimension two of the local water depth  $d/L_0$ .



288  
289  
290

**Figure 6a:**Vertical elevation  $\eta_a(d/L_0, \beta)$  of the sea surface in the shoaling zone in 3D as a function of the local water depth  $d/L_0$  and the seabed slope  $\beta$ .



291  
292  
293  
294

**Figure 6b:** Vertical elevation of the marine surface offshore  $\eta_o(d/L_0)$  and in the shoaling zone  $\eta_a(d/L_0, \beta = 0,05)$  in 3D of the local water depth  $d/L_0$ .

295

### 3.2. DISCUSSION

296

297

298

299

300

301

302

303

304

305

306

307

308

309

310

311

312

313

314

315

316

317

318

319

320

321

322

323

324

325

326

327

328

➤ It is important to note that the amplitude of the speed decreases exponentially with a coefficient proportional to the wave number  $k$ . Therefore, the orbital speed of waves with a larger period (smaller number of waves) will be more present at the bottom than that of waves with short periods (**Figures 3a** and **3b**). The waves induce an orbital movement in the water and the amplitude of this movement decreases with depth (**Figures 3a** and **3b**). In shallow water, the elliptical paths followed by water particles flatten to horizontal lines, particularly at the bottom, where there is no vertical flow. The trajectory of the particles is therefore circular in infinite depth (offshore) and elliptical becomes more and more crushed as the bottom rises.

➤ **Figure 4.I** indicate a strong temporal variability of  $H_s$  extending from typical wind force values (minimum  $0.71 m$ ) to fairly energetic swells (maximum  $3.22 m$ ) during the years 2015 and 2016, some sequences exceptionally energetic with significant height values between  $3.05$  and  $3.22 m$ . This mixture of ocean regime and sea wind is corroborated by the maximum swell periods observed, varying between  $5.50$  and  $15.66 s$  (**Figure 4.II**). The observed wave peak periods vary between  $4.38$  and  $17.85 s$  with an average of  $11.7 s$ . The maximum direction of all waves varies very little (standard deviation of  $2.38^\circ$ ) with an average direction of  $211.5^\circ$  clockwise from the north (dominant waves from the SSW sector) except on rare occasions ( $266$  and  $235^\circ$  respectively in 2015 and 2016, (**Figure 4.III**, we see a different grid ( $3,15^\circ > 1,7^\circ$ ). The average height of all waves over the period (2015-2016). is  $1.29 m$  and  $9.30 m$  for the peak period. The analysis of the different curves (**Figure 4**) of the wave parameters makes it possible to identify two phases: the first going from June to July characterized by waves of fairly strong energy ( $H_{smoy} > 1,32 m$  and  $T_{pmoy} > 11 s$ ). The second phase goes from July to August, it is characterized by slightly less energetic waves ( $H_{smoy} < 1,1 m$  and  $3,4 s < T_p < 16 s$ ). The wave periods during the first phase are as high as the significant heights. In contrast, in the second phase, the wave height decreased with the increase in wind speed [2]. The waves are therefore characterized by energy spectra, which reveal characteristic quantities, with for example a significant height  $H_s$ , a significant period  $T_s$ , etc.... These spectra are broad for wind waves, and narrower for an already formed swell which continues to propagate far from its zone of generation by the wind.

➤ In **Figures 5a, 5b**, it is noted that the calculated results for the depth water wave profile for linear waves are quite similar to nonlinear waves, thus the comparisons indicate that the currently obtained solutions deviate from the existing results of Cruz et al for regular linear waves, so some anomaly is expected between the present results and Cruz's solutions formulated for nonlinear waves. Water particle velocities under linear waves are greatest at the surface and decrease in magnitude with depth (**Figures 5c** and **5d**). The speed of wave propagation depends on their

329 wavelength, their amplitude, and as they approach the coastline, the water depth (**Figures 5c**  
330 and **5d**). The phenomenon of wave propagation is therefore dispersive. Furthermore, the waves do  
331 not all propagate in the same direction, resulting in a sometimes chaotic appearance of the sea  
332 surface state. The directions of particle speeds are linked to the movement of the water  
333 surface. At the crest of the wave, the movement of the water is horizontal and in the direction of  
334 the wave. At the trough, the speed is reversed (by the same magnitude as at the peak in linear  
335 theory). Vertical velocities reach their maximum when water crossings occur. We notice that the  
336 velocities of the water particles increase (**Figures 5c** and **5d**) and the accelerations of the water  
337 particles decrease (**Figures 5e** and **5f**) from deep water to shallow water, this gives us a good  
338 agreement between these results and previous results for deep-water and shallow-water wave  
339 measurements. It can be said from the results obtained that the wave height has a considerable  
340 effect on the wave profile. Then, the crest has moved, the pressure is maximum at its summit and  
341 decreases going down in the direction of propagation (**Figure 5j**). The pressure decreases, so the  
342 speed increases. On the other hand, in the left part of the direction of propagation, the pressure  
343 increases from left to right (up to the trough), the pressure force acting under the wave crest is  
344 greater than the pressure force under the wave trough leading to a net effort over a wave period  
345 (**Figure 5j**). **Figures 5a, 5b, 5c, 5d, 5e, 5f, 5g, 5h**, show a good agreement between the speeds  
346 and accelerations of the current model, there is only a difference in the values.

347 ➤ The analysis of the results, after several years of monitoring the morphodynamics of the  
348 Beninese beach, made it possible to highlight the link between the sea surface and the  
349 seabed. However, these results should be moderated due to the particularly favorable weather  
350 conditions (absence of erosive storms) observed since 2011. In the breaking zone where  $d = 3m$ ,  
351 this potential also varies with a non-negligible average. The shoaling zone is therefore a zone of  
352 strong amplification of the energy power of the swell, while those of Surf and Swash are the  
353 zones of energy dissipation. These results show that the swells in Benin are more energetic in  
354 the shoaling zone. The curves of **Figures 6, 6a, and 6b**, translate the variations of the vertical  
355 elevation of the free surface of the ocean according to the local water depth. Note that the curve  
356 of **Figure 6** represents dimension 2 (2D) while those of **Figures 6a** and **6b** are its representations  
357 in dimension 3 (3D). They confirm:

- 358 - The constancy of the various offshore parameters.
- 359 - Height amplification crest to the trough of the swells in the shoaling zone under the  
360 disturbing effect of the seabed.

361 The slope of this seabed causes the decrease or contraction of the wavelength. The curve of  
362 **Figure 6b**, which represents the variations of the vertical elevation of the free surface of the  
363 ocean according to the local water depth  $d = \mu L_o$  and the slope of the seabed  $\beta$  in the shoaling  
364 zone, reveals that the randomness accompanied by small oscillations on the surface of the swell  
365 is due to the variability of the slope of the seabed.

#### 367 4. CONCLUSION

368 In the Gulf of Guinea at Cotonou, the swells are regular and have a constant average  
369 height  $H_o = 0,8m$  and an average period  $T = 11s$  in deep waters. In the coastal zone, the disturbing  
370 effect of the seabed causes them to rise to the breaking point and it is the modified Boussinesq  
371 theory, proposed by Peregrine in 1967, makes it possible to model them. These swells become  
372 very energetic in this zone, their height is amplified and remains proportional to  $(d^{-1/4})$ . At the  
373 breaking point, the maximum height these swells reach varies between  $1,7m$  and  $2,5m$ . Their  
374 bathymetric surge, occurs at a position where the local water depth  $d_p$  oscillates between  $1.6m$   
375 and  $4.5m$  very close to the coastline depending on the value of the slope of the seabed. This  
376 Breaking is a sudden energy discharge that induces and accentuates the phenomenon of coastal  
377 erosion. The waves are therefore characterized by energy spectra, which reveal characteristic  
378 quantities, with for example a significant height  $H_s$ , a significant period  $T_s$ , etc.... These spectra are  
379 broad for wind waves, and arrower for an already-formed swell which continues to propagate far  
380 from its zone of generation by the wind. Swells induce an orbital motion in the water and the  
381 amplitude of this motion decreases with depth. It is important to note that the amplitude of the

382 velocity decreases exponentially with a coefficient proportional to the number of waves  $k$ . So, the  
383 orbital velocity of swells with a longer period (smaller wave number) will be more present at sea  
384 floor than that of waves with shorter periods. The propagation velocity of the swells depends on  
385 their wavelength, their amplitude and when approaching the coast, the water depth. The swells  
386 are therefore characterized by energy spectra, which show characteristic quantities, with for  
387 example a significant height  $H_s$ , a significant period  $T_s$ , etc. Water particles also describe vertical  
388 circles which become progressively smaller with increasing depth, the decrease being  
389 exponential. The reason for describing simple waves is that they represent the basic solutions of  
390 the physical equations that govern waves on the sea surface and they are the building blocks for  
391 real wave fields occurring at sea. Actually, the idea of basic sinusoidal waves is widely applied to  
392 help in the comprehension and characterization of waves. Despite this simplified description,  
393 definitions and formulas derived from waves are intensively employed in practice and have  
394 proven their value. It can be said from the results obtained that the wave height has a  
395 considerable effect on the wave profile. It has a major impact on the wave and its constituent  
396 parts, as seen by the fluctuation in water depth as a function of distance from the bed. From the  
397 present work we can say that the combination of the effects of height and depth together  
398 contribute to the understanding of the behavior of the wave and its velocities and accelerations of  
399 the water particles. Therefore, the orbital speed of waves with a larger period (smaller number of  
400 waves) will be more present at the bottom than that of waves with short periods. The speed of  
401 wave propagation depends on their wavelength, their amplitude, and as they approach the coast,  
402 the water depth. The phenomenon of wave propagation is therefore dispersive. Furthermore, the  
403 waves do not all propagate in the same direction, resulting in a sometimes chaotic appearance of  
404 the sea surface. The variation in the depth of the water as a function of the distance from the bed  
405 shows that it has a very significant effect on the wave and its components. Wave propagation is a  
406 phenomenon that is very sensitive to a large number of parameters, in particular, the speed of  
407 the waves after breaking  $v_g$ , their period  $T$ , their wavelength in deep waters  $L_0$ , the slope of the  
408 seabed  $\beta$ , the crest to trough height of the swell  $H$ , the obliquity of the swell  $\alpha$ , the local water  
409 depth  $d$  . . .

410

#### 411 **ACKNOWLEDGEMENTS**

412 The authors thank the Beninese Center for Scientific Research and Innovation  
413 (IRHOB/CBRSI) not only for supporting this research work but also for the data made  
414 available to us.

415

#### 416 **AUTHORS CONTRIBUTIONS**

417 This work was carried out in collaboration between the author and all co-authors. "The main  
418 author" and the "first three co-authors" designed the study, performed the statistical analysis, and  
419 wrote the protocol and the first draft of the manuscript. The "last co-author" supervised and  
420 coordinated the work. The other co-authors performed the calculations and analyses of the study.  
421 All co-authors read and gave final approval for publication.

422

#### 423 **CONFLICT OF INTEREST**

424 The authors state that there were no financial or commercial relationships that may be seen as  
425 having a conflict of interest when conducting the research.

426

#### 427 **DATA AVAILABILITY**

428 The datasets generated during and/or analyzed during the current study are available from the  
429 authors at reasonable request.  
430 Disclaimer (Artificial intelligence)

431 Option 1:

432 Author(s) hereby declare that NO generative AI technologies such as Large Language  
433 Models (ChatGPT, COPILOT, etc) and text-to-image generators have been used during  
434 writing or editing of manuscripts.

435 Option 2:

436 Author(s) hereby declare that generative AI technologies such as Large Language Models,  
437 etc have been used during writing or editing of manuscripts. This explanation will include  
438 the name, version, model, and source of the generative AI technology and as well as all  
439 input prompts provided to the generative AI technology

440 Details of the AI usage are given below:

441 1.

442 2.

443 3.

444

445

446

447

#### REFERENCES

- 448 [1] N. B. TOKPOHOZIN, « INFLUENCE DE LA HOULE SUR LA DYNAMIQUE  
449 SEDIMENTAIRE DANS LA ZONE CÔTIÈRE DU BENIN », Thèse de doctorat Unique,  
450 Université d'Abomey-Calavi (UAC), Institut de Mathématiques et de Sciences Physiques  
451 (IMSP), 2016.
- 452 [2] B. N. Tokpohozin *et al.*, « Prospects for the Characterization of the Fundamental  
453 Parameters Linked to the Energy Spectrum of the Aeolian Sea State in Benin Coastal  
454 Zone », *Curr. J. Appl. Sci. Technol.*, vol. 42, n° 42, p. 19-35, nov. 2023, doi:  
455 10.9734/cjast/2023/v42i424270.
- 456 [3] Z. N. Al-Dwairi, K. Y. Tahboub, N. Z. Baba, C. J. Goodacre, et M. Özcan, « A Comparison  
457 of the Surface Properties of CAD/CAM and Conventional Polymethylmethacrylate  
458 (PMMA) », *J. Prosthodont.*, vol. 28, n° 4, p. 452-457, avr. 2019, doi: 10.1111/jopr.13033.
- 459 [4] G. Hervé Houngué, B. B. Kounouhewa, R. Almar, Z. Sohoun, J.-P. Lefebvre, et M.  
460 Houépkonhéha, « Waves Forcing Climate on Bénin Coast, and the Link with Climatic Index,  
461 Gulf of Guinea (West Africa) », *J. Coast. Res.*, vol. 81, n° sp1, p. 130, sept. 2018, doi:  
462 10.2112/SI81-017.1.
- 463 [5] N. B. Tokpohozin, B. Kounouhewa, G. Y. H. Avoisevou, A. Houekpoheham, et C. N.  
464 Awanou, « Modelling of sediment movement in the surf and swash zones », *Acta Oceanol.  
465 Sin.*, vol. 34, n° 2, p. 137-142, févr. 2015, doi: 10.1007/s13131-015-0610-2.
- 466 [6] R. Almar *et al.*, « The Grand Popo beach 2013 experiment, Benin, West Africa: from short  
467 timescale processes to their integrated impact over long-term coastal evolution », *J. Coast.  
468 Res.*, vol. 70, p. 651-656, avr. 2014, doi: 10.2112/SI70-110.1.
- 469 [7] O. G. Acclassato, N. B. Tokpohozin, C. D. Akowanou, A. M. Houépkonhéha, G. H. Houngue,  
470 et B. B. Kounouhéwa, « Study of Dissipating of Wave Energy in the Breakers Zone of the  
471 Gulf of Guinea: Case of Autonomous Port of Cotonou in Benin Coastal Zone », *J. Mod.  
472 Phys.*, vol. 13, n° 09, p. 1272-1286, 2022, doi: 10.4236/jmp.2022.139076.

- 473 [8] T. Noukpo Bernard, F. Jean-Louis C., H. H. Guy, H. A. Mathias, et K. B. Basile,  
474 « ENERGETIC POWER ESTIMATION OF SWELLS AND ORBITAL MARINE CURRENTS  
475 IN BENIN COASTAL ZONE (GULF OF GUINEA) », *Int. J. Adv. Res.*, vol. 11, n° 02, p.  
476 366-382, févr. 2023, doi: 10.21474/IJAR01/16261.
- 477 [9] A. Melet, R. Almar, M. Hemer, G. Le Cozannet, B. Meyssignac, et P. Ruggiero,  
478 « Contribution of Wave Setup to Projected Coastal Sea Level Changes », *J. Geophys. Res.*  
479 *Oceans*, vol. 125, n° 8, p. e2020JC016078, août 2020, doi: 10.1029/2020JC016078.
- 480 [10] G. H. Houngouè, M. A. Houépkonhéha, N. B. Tokpohozin, et B. B. Kounouhéwa, « Wave  
481 Energy Potential Assessment during Recent Extreme Events Observed on Benin's Coastal  
482 Area, Gulf of Guinea (West Africa). », *Journal de physique de la SOAPHYS*, Afrique de  
483 l'Ouest, p. 1 (2019) C19A15, 2019.
- 484 [11] G. H. Houngouè, B. B. Kounouhéwa, M. A. Houépkonhéha, B. N. Tokpohozin, et V. I.  
485 Madogni, « Wave Energy Resources Assessment Offshore Benin from ERA Re-Analysis:  
486 Gulf of Guinea », *Phys. Sci. Int. J.*, vol. 19, n° 4, p. 1-11, nov. 2018, doi:  
487 10.9734/PSIJ/2018/44226.
- 488 [12] N. B. Tokpohozin, J.-L. Fannou, A. M. Houekpohéha, H. G. Houngouè, et B. B.  
489 Kounouhéwa, « STATISTICAL STUDY OF WAVE PARAMETERS : SEA STATES IN THE  
490 DEEP WATERS (OFFSHORE) OF THE GULF OF GUINEA IN BENIN », *Int. J. Curr. Res.*,  
491 vol. Vol. 15, n° Issue, 02, p. pp.23709-23719, févr. 2023, doi: 10.24941/ijcr.44701.02.2023.
- 492 [13] M. Rabaud et F. Moisy, « The Kelvin–Helmholtz instability, a useful model for wind-wave  
493 generation? », *Comptes Rendus Mécanique*, vol. 348, n° 6-7, p. 489-500, nov. 2020, doi:  
494 10.5802/crmeca.31.
- 495 [14] Aurélien BABARIT, Jean-Marc ROUSSET, Hakim MOUSLIM, Judicaël AUBRY, Hamid  
496 BEN AHMED, et Bernard MULTON, « Chapter 4 Wave Prediction Models », in *Elsevier*  
497 *Oceanography Series*, vol. 49, Elsevier, 1989, p. 75-105. doi: 10.1016/S0422-  
498 9894(08)70124-7.
- 499 [15] M. Clauss, C. Nunn, J. Fritz, et J. Hummel, « Evidence for a tradeoff between retention time  
500 and chewing efficiency in large mammalian herbivores », *Comp. Biochem. Physiol. A. Mol.*  
501 *Integr. Physiol.*, vol. 154, n° 3, p. 376-382, nov. 2009, doi: 10.1016/j.cbpa.2009.07.016.
- 502 [16] D. Chalikov et D. Sheinin, « Modeling extreme waves based on equations of potential flow  
503 with a free surface », *J. Comput. Phys.*, vol. 210, n° 1, p. 247-273, nov. 2005, doi:  
504 10.1016/j.jcp.2005.04.008.
- 505 [17] D. Isebe *et al.*, « Une nouvelle approche pour la protection des plages : Application à la  
506 plage du Lido de Sète », in *Xèmes Journées, Sophia Antipolis*, Editions Paralia, 2008, p.  
507 263-272. doi: 10.5150/jngcgc.2008.025-1.
- 508 [18] G. Chen, B. Chapron, R. Ezraty, et D. Vandemark, « A global view of swell and wind sea  
509 climate in the ocean by satellite altimeter and scatterometer. », *Journal of atmospheric and*  
510 *Oceanic Technology*, p. 1849-1859, 2002.
- 511 [19] Y. Xu et X. Yu, « Enhanced formulation of wind energy input into waves in developing  
512 sea », *Prog. Oceanogr.*, vol. 186, p. 102376, juill. 2020, doi:  
513 10.1016/j.pocean.2020.102376.
- 514 [20] J.-H. G. M. Alves, « Numerical modeling of ocean swell contributions to the global wind-  
515 wave climate », *Ocean Model.*, vol. 11, n° 1-2, p. 98-122, janv. 2006, doi:  
516 10.1016/j.ocemod.2004.11.007.
- 517 [21] G. M. A. Jose-Henrique, « Numerical modeling of ocean swell contributions to the global  
518 wind-wave climate », *Ocean Modelling*, p. 98-122, 2006.
- 519 [22] B. Castelle, P. Bonneton, H. Dupuis, et N. Sénéchal, « Double bar beach dynamics on the  
520 high-energy meso-macrotidal French Aquitanian Coast: A review », *Mar. Geol.*, vol. 245, n°  
521 1-4, p. 141-159, nov. 2007, doi: 10.1016/j.margeo.2007.06.001.
- 522 [23] R. M. Castelao, « Mesoscale eddies in the South Atlantic Bight and the Gulf Stream  
523 Recirculation region: Vertical structure », *J. Geophys. Res. Oceans*, vol. 119, n° 3, p.  
524 2048-2065, mars 2014, doi: 10.1002/2014JC009796.

- 525 [24] Q. Liu *et al.*, « Observation-Based Source Terms in the Third-Generation Wave Model  
526 WAVEWATCH III: Updates and Verification », *J. Phys. Oceanogr.*, vol. 49, n° 2, p.  
527 489–517, févr. 2019, doi: 10.1175/JPO-D-18-0137.1.
- 528 [25] V. G. Polnikov, « The role of wind waves in dynamics of the air-sea interface », *Izv.*  
529 *Atmospheric Ocean. Phys.*, vol. 45, n° 3, p. 346–356, juin 2009, doi:  
530 10.1134/S0001433809030086.
- 531 [26] A. Zavadsky, D. Liberzon, et L. Shemer, « Statistical Analysis of the Spatial Evolution of the  
532 Stationary Wind Wave Field », *J. Phys. Oceanogr.*, vol. 43, n° 1, p. 65–79, janv. 2013, doi:  
533 10.1175/JPO-D-12-0103.1.
- 534